Chaos-Assisted Long-Range Tunneling for Quantum Simulation

Maxime Martinez,[1] Olivier Giraud,[2] Denis Ullmo,[2] Juliette Billy,[3] David Guéry-Odelin,[3] Bertrand Georgeot,[1] and Gabriel Lemarié[1,4,5]

[1]*Laboratoire de Physique Théorique, Université de Toulouse, CNRS, UPS, 31062 Toulouse France*
[2]*Université Paris-Saclay, CNRS, LPTMS, 91405 Orsay, France*
[3]*Laboratoire Collisions Agrégats Réactivité, Université de Toulouse, CNRS, UPS, 31062 Toulouse France*
[4]*MajuLab, CNRS-UCA-SU-NUS-NTU International Joint Research Unit, 117543 Singapore*
[5]*Centre for Quantum Technologies, National University of Singapore, 117543 Singapore*

(Received 3 November 2020; revised 2 March 2021; accepted 29 March 2021; published 28 April 2021)

We present an extension of the chaos-assisted tunneling mechanism to spatially periodic lattice systems. We demonstrate that driving such lattice systems in an intermediate regime of modulation maps them onto tight-binding Hamiltonians with chaos-induced long-range hoppings $t_n \propto 1/n$ between sites at a distance n. We provide a numerical demonstration of the robustness of the results and derive an analytical prediction for the hopping term law. Such systems can thus be used to enlarge the scope of quantum simulations to experimentally realize long-range models of condensed matter.

DOI: 10.1103/PhysRevLett.126.174102

Introduction.—In recent years, there has been considerable interest in the quantum simulation of more and more complex problems of solid state physics [1–3]. In this context, lattice-based quantum simulation has become a key technique to mimic the periodicity of a crystal structure. In such systems, the dynamics is governed by two different types of processes: hopping between sites mediated by a tunneling effect and interaction between particles. While several ways exist to implement long-range interactions [4–7], long-range hoppings have been up to now very challenging to simulate [8,9]. These long-range hoppings, however, have aroused great theoretical interest in condensed matter, as they are associated with important problems such as glassy physics [10], many-body localization [11], and quantum multifractality [12]. In this Letter, we show that such long-range tunneling can be engineered in driven lattices in a moderate regime of modulation.

Temporal driving techniques are widely used in quantum simulation [13], as fast driving can lead to new topological effects [14–18] and strong driving can mimic disorder [19–24]. In the intermediate regime we focus on, cold atoms in driven lattices have a classical dynamics that is neither fully chaotic (a case first explored in [25]) nor regular (corresponding to the fast driving case). As for most real-life systems, the phase space representation of their dynamics shows the coexistence of chaotic and regular zones. Our main result is based on the richness of the quantum tunneling, known to be "chaos-assisted" in such systems [26–38]. This phenomenon is well understood between two regular islands, where it translates into large resonances of the tunneling rate between the two islands when varying a system parameter. Chaos-assisted tunneling has been observed in different experimental contexts with electromagnetic waves [30,39–44] or cold atoms [45–48] (see also [49–52] for other related experiments).

In this Letter, we address the generalization of chaos-assisted tunneling (CAT) to *mixed lattices* of regular islands embedded in a chaotic sea obtained in a moderate regime of temporal driving. We show that, remarkably, such a dynamical quantum system can be mapped onto an effective tight-binding Hamiltonian with long-range hoppings $\propto 1/n$, with n the distance between sites. Beyond the intrinsic interest of a new observable quantum chaos effect, our results open new engineering possibilities for lattice-based quantum simulations as they are highly generic, accessible for state-of-the-art experiments, and species independent (in a cold atom context).

Model.—We consider an experimental situation similar to [48], i.e., a condensate of cold atoms in an optical lattice whose intensity is time-modulated periodically [25,36,45–47,53]. As in [48], we assume a low density such that interactions are negligible. Using dimensionless variables [54], the dynamics is given by the single particle Hamiltonian

$$H(x,t) = \frac{p^2}{2} - \gamma(1 + \varepsilon \cos t)\cos x. \tag{1}$$

γ is the dimensionless depth of the optical lattice and ε the modulation amplitude, with dimensionless time period $T = 2\pi$ and spatial period $\lambda = 2\pi$. The effective Planck constant $\hbar_{\text{eff}} = -i[x,p] = 2E_L/h\nu$ can be tuned experimentally (ν is the modulation frequency and $E_L = h^2/2md^2$ a lattice characteristic energy, with d the lattice spacing and m the atomic mass). Beyond this model, our

 © 2021 American Physical Society

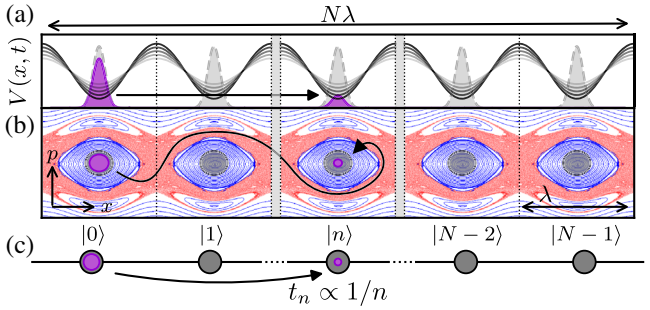

FIG. 1. Three representations of CAT in a driven lattice. (a) *In situ* description: a wave function tunnels between potential wells. (b) Phase space description: the wave function escapes from a stable island (blue) by regular tunneling, spreads in the chaotic sea (red), and tunnels in another island. (c) Tight-binding description: the system contains N sites with coupling between the ith and jth sites proportional to $1/|i-j|$.

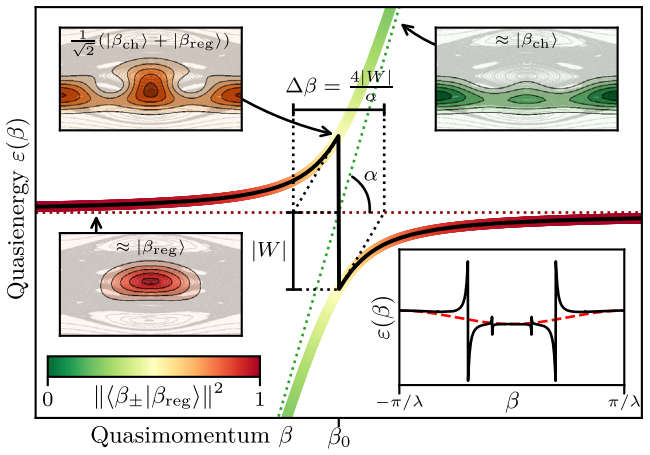

FIG. 2. In a mixed lattice as in Fig. 1, a CAT resonance between a regular Bloch wave $|\beta_{reg}\rangle$ and a chaotic one $|\beta_{ch}\rangle$ leads to a discontinuity in the energy band of the associated tight-binding model (solid black line). The main panel shows the avoided crossing characterized by $|W|$ (the strength of the coupling between $|\beta_{reg}\rangle$ and $|\beta_{ch}\rangle$), α (the slope of the energy of $|\beta_{ch}\rangle$), β_0 (the point of equal mixing), and $\Delta\beta$ (the crossing width). Near $\beta = \beta_0$, the eigenstates $|\beta_\pm\rangle$ become a mixture of $|\beta_{reg}\rangle$ and $|\beta_{ch}\rangle$. The color code gives the intensity of the mixing (projection on $|\beta_{reg}\rangle$). Husimi representations [56–58] of $|\beta_\pm\rangle$ are on top of the classical dynamics phase portrait. Inset: black solid line is the effective regular band and red dashed line a nearest-neighbor approximation with parameters extracted from the effective regular band at $\beta = 0$ and $\beta = \pi/\lambda$ ($\hbar_{eff} = 0.4, \gamma = 0.20, \epsilon = 0.15$).

results are valid for almost any modulation waveform (e.g., phase modulation or kicked potentials).

Semiclassical picture.—The classical dynamics of this time-periodic system is best viewed through a stroboscopic phase space, using values of (x, p) at each modulation period $t = jT$, j integer. For $\varepsilon = 0$, the system is integrable. When ε increases, chaos develops, forming a chaotic sea that surrounds regular islands of orbits centered on the stable points ($x = 2n\pi$, $p = 0$, n an integer) of the potential wells (see Fig. 1). At $\varepsilon = 0$, with no chaotic sea, tunneling essentially occurs between adjacent wells, and the system can be described for deep optical lattices by an effective tight-binding Hamiltonian with nearest-neighbor hopping. Our main objective is to describe in a similar way the modulated system, a dynamical, spatially periodic lattice of N regular islands indexed by $n \in [\![0, N-1]\!]$, surrounded by a chaotic sea.

In a stroboscopic point of view, the quantum dynamics is described by the evolution operator U_F over one period. Each eigenstate $|\phi_l\rangle$ of U_F is associated with a quasienergy ε_l, so that $U_F|\phi_l\rangle = \exp(-i\varepsilon_l T/\hbar_{eff})|\phi_l\rangle$. Equivalently, the Hamiltonian $H_{strob} \equiv i(\hbar_{eff}/T)\log U_F$ gives the same stroboscopic dynamics as U_F and has the same eigenstates $|\phi_l\rangle$ with energies ε_l.

In the semiclassical regime where $\hbar_{eff} < \mathcal{A}$, with $\mathcal{A}$ the area of a regular island, the quantum dynamics is strongly influenced by the structures of the classical phase space. Quantum eigenstates can be separated into two types [27,55]: regular (localized on top of regular orbits) or chaotic (spread over the chaotic sea) (see Fig. 2).

The tunnel coupling between regular states is well understood for $N = 2$ regular islands surrounded by a chaotic sea (original CAT effect [26,27]). With no chaotic sea, tunneling involves only a doublet of symmetric and antisymmetric states. In the presence of a chaotic sea, CAT is a 3-level mechanism with one of the regular states interacting resonantly with a chaotic state. This coupling leads to an energy shift and thus to a strong variation of the energy splitting giving the tunneling frequency. These CAT resonances, observed in a quantum system only recently [48], occur quite erratically when varying a system parameter [26,28]. The CAT process involves a purely quantum transport (tunneling to the chaotic sea) and a classically allowed transport (diffusion in the chaotic sea). Thus in mixed lattices, long-range tunneling can be expected since the chaotic sea connects all the regular islands across the lattice (see Fig. 1).

Effective Hamiltonian.—The existence of regular islands in the center of each cell motivates the introduction of a set of regular states $\{|n_{reg}\rangle\}$ (whose exact construction [30] is not crucial for our discussion) localized on these islands and forming a lattice. For simplicity, we work in the regime $\hbar_{eff} \lesssim \mathcal{A}$ with only one regular state per island. In contrast to regular lattices, where tunneling couples only neighboring sites, there exists an *indirect* coupling between distant islands of the modulated lattice mediated by the delocalized chaotic states. As in the original CAT scenario, we can expect the overlap with the chaotic sea to remain small at any time. This motivates us to capture the physics of tunneling in our system through an effective Hamiltonian H_{eff} acting only in the regular subspace but generating the same dynamics as H_{strob} in this subspace [59–61]. Thus, the

effective quantum propagator $(E - H_{\text{eff}})^{-1}$ (Green's function at energy E) should be equal to the exact one projected onto the regular subspace $P_{\text{reg}}(E - H_{\text{strob}})^{-1}P_{\text{reg}}$. The main consequence of this relation is that the effective spectrum of H_{eff} should be included in that of H_{strob} (see below). Thus, in the effective picture, coupling with chaotic states simply translates into a shift of the energy of each regular Bloch state $|\beta_{\text{reg}}\rangle = (1/\sqrt{N})\sum_n \exp(i\beta\lambda n)|n_{\text{reg}}\rangle$ (with β an integer multiple of $2\pi/\lambda N$). The resulting dressed regular band $\varepsilon^{\text{eff}}_{\text{reg}}(\beta)$ then gives access to the effective tunneling coupling $t^{\text{eff}}_n \equiv \langle (m+n)_{\text{reg}}|H_{\text{eff}}|m_{\text{reg}}\rangle$ through the Fourier transform in quasimomentum:

$$t^{\text{eff}}_n = \frac{1}{N}\sum_{\beta} \varepsilon^{\text{eff}}_{\text{reg}}(\beta)\exp(i\beta\lambda n). \tag{2}$$

The simplest way to determine the effective spectrum is to choose the N most relevant energies in the full exact spectrum. The natural choice is to select energies of eigenstates with the largest projection on the regular subspace. In *mixed lattices*, this gives systematic discontinuities in the effective band due to accidental degeneracies between a regular $|\beta_{\text{reg}}\rangle$ and a chaotic state $|\beta_{\text{ch}}\rangle$. Close to such avoided crossings, the branch giving the effective regular energy changes, giving a sharp discontinuity of $\varepsilon^{\text{eff}}_{\text{reg}}(\beta)$ (see Fig. 2). These discontinuities cause, from the Fourier transform in Eq. (2), a long-range decay of the effective coupling term $t^{\text{eff}}_n \sim 1/n$ (see Fig. 5).

The two main features of these resonances come from the mixed nature of the system (see Fig. 2): (i) They are sharp because the local slope α of the crossing state is large, the chaotic states being delocalized, and thus sensitive to boundary conditions. (ii) Their heights $2|W|$ are larger than the regular band width (nearest-neighbor hopping amplitudes in the regular case $\varepsilon = 0$).

Numerical simulations.—To test the accuracy of this effective tight-binding picture, we compare the exact stroboscopic dynamics with the one given by the effective Hamiltonian, considering a wave packet initially localized on a single regular island of the modulated lattice (see [62] for details). As concerns the exact dynamics, the initial condition was chosen to be a localized (Wannier) state of the undriven lattice ($\varepsilon = 0$) in the regular island $n_0 = (N-1)/2$, N being odd. We also used the localized states $|n_{\text{reg}}\rangle$ to estimate the projection of the wave function on the chaotic layer through $P_{\text{ch}} \equiv 1 - P_{\text{reg}}$. The effective dynamics was studied by propagation of a state initially located at the site n_0 with the effective Hamiltonian. In both simulations, we used a local observable $\hat{p}_n$ which probes the probability at each site, defined as $\hat{p}_n \equiv |n\rangle\langle n|$ in the effective system, $\hat{p}_n \equiv \int_{n\lambda}^{(n+1)\lambda} |x\rangle\langle x|\mathrm{d}x$ in the exact one (this choice ensures that $\sum_n \hat{p}_n = \mathbb{1}$ in both cases), and a global observable $\widehat{\Delta n^2} = \sum_n (n-n_0)^2\hat{p}_n$ to estimate the spreading of the wave function.

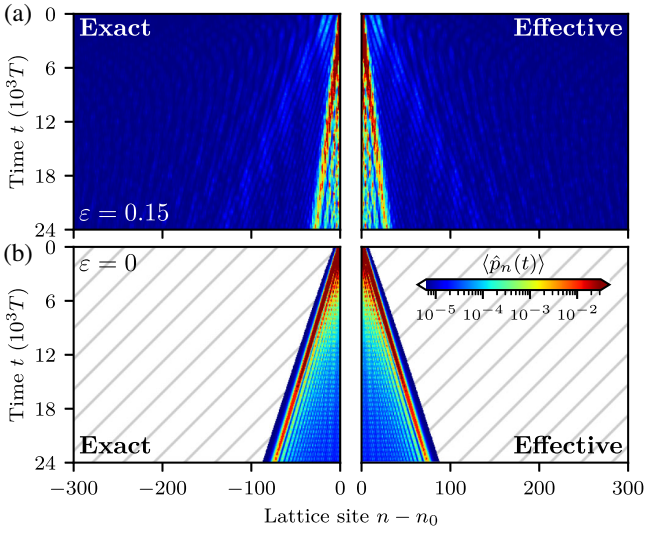

FIG. 3. Dynamics of a wave packet initially located on a single regular island or site n_0. Color plot of the time evolution of the spatial probability distribution, with $\gamma = 0.2$, $\hbar_{\text{eff}} = 0.4$, and $\varepsilon = 0.15$ for the modulated lattice (a) or for the unmodulated lattice, i.e., $\varepsilon = 0$ (regular case) (b). The exact dynamics (left) is compared to the corresponding effective description (right). Note that the system is symmetric through $n - n_0 \to n_0 - n$.

We simulated different system sizes up to $N = 1079$ with periodic boundary conditions and found a very good agreement between the two approaches (see Figs. 3 and 4 and [62] for additional results). In the modulated case, there is a fast and long-range spreading of the wave function [Fig. 3(a)], in particular long tails of the spatial distribution [Fig. 4(a)] that is responsible for the tremendous growth of the standard deviation [Fig. 4(c)]. The standard deviation saturates with a strong finite size effect, an additional signature of the long-range tunneling. In contrast, the regular $\varepsilon = 0$ case gives a slow, short-range ballistic spreading of the wave function with no finite-size effect [Figs. 3(b) and 4(c)].

Analytical derivation of the hopping law.—In addition to the expected long-range decay $\propto 1/n$ of the effective coupling term, numerical simulations show fluctuations around this algebraic law (see Fig. 5). We can explain them with a simple model. For each of the N_{res} resonances in the effective band, we apply a two-level model with only three parameters (see Fig. 2): the slope $\alpha = \mathrm{d}\varepsilon_{\text{ch}}/\mathrm{d}\beta$ of the energy of a chaotic state with β, the coupling intensity W between chaotic and regular states, and the position β_0 of the crossing in the spectrum. Using the linearity of Eq. (2) and assuming sharp resonances ($\Delta\beta \ll 2\pi/\lambda$), the asymptotic behavior of t^{eff}_n is (see [62])

$$t^{\text{eff}}_n \approx \frac{i}{\pi n}\sum_{\text{resonances}} \text{sgn}(\alpha)|W|\mathrm{e}^{in\beta_0\lambda}. \tag{3}$$

This model is in very good agreement with numerical data (see Fig. 5 and [62]) and shows that the relevant timescale

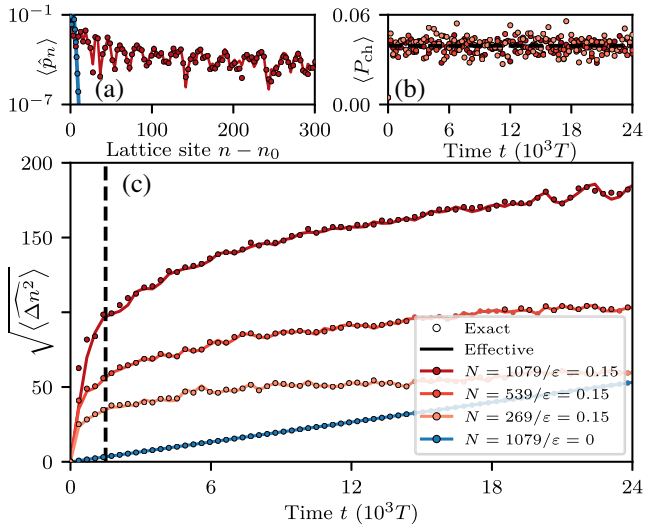

FIG. 4. Characterization of the dynamics of a wave packet initially located on a single regular island or site n_0 (corresponding to Fig. 3). (a) Spatial probability distribution of the wave packet after $t = 1500$ T. (b) Overlap of the wave function with the chaotic sea vs time (see text). (c) Standard deviation of the spatial distribution vs time. Symbols are for the exact dynamics and solid lines for the effective dynamics. Red data correspond to modulated lattices with different sizes, and blue data correspond to the unmodulated lattice (regular case).

of the tunneling dynamics is $\hbar_{\rm eff}/|W|$. The phase term $e^{in\beta_0\lambda}$, which depends on the position of the resonances in the effective band, gives the observed fluctuations of hopping amplitudes around the algebraic law.

Since the W's of the $N_{\rm res}$ resonances are associated with tunnel coupling to chaotic states, random matrix theory suggests that they can be described as independent

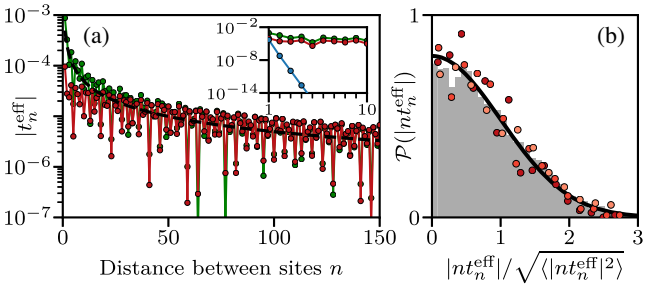

FIG. 5. (a) Effective hopping amplitude $|t_n^{\rm eff}|$ vs distance between sites n for $\gamma = 0.2$, $\varepsilon = 0.15$, and $\hbar_{\rm eff} = 0.4$. Red data were extracted from numerical Fourier series of the effective band structure. Green data correspond to Eq. (3) with parameters extracted from the band structure. Black solid line is the typical value of Eq. (3) (without the phase term). Inset: small-distance behavior and additional blue data for unmodulated case $\varepsilon = 0$. (b) Distribution of fluctuations around the $1/n$ law for five parameter sets: histogram corresponds to cumulative values for $1500 < n < 10\,000$, dots are partial datasets of 500 consecutive values of n, and black curve is analytical prediction (see text).

Gaussian variables with a fixed variance w^2. In the same spirit, as soon as n is large enough, the phases $n\beta_0\lambda$ mod $[2\pi]$ can be considered random. Using the known results about sums of complex numbers with Gaussian amplitudes and random phases [63], Eq. (3) leads to a simple statistical model for the couplings, with $|t_n^{\rm eff}| \equiv \mathcal{W}/n$ with $\mathcal{W}$ a Gaussian random variable of variance $N_{\rm res}w^2$. We stress that this implies the distribution of $n|t_n^{\rm eff}|$ is universal. Figure 5(b) shows the validity of this approach.

Discussion.—The theoretical results presented above rely on the effective Hamiltonian picture. It is thus important to assess its validity in our context. The exact tunneling dynamics between two sites can be written $\langle(n+m)_{\rm reg}|U_F|m_{\rm reg}\rangle = (1/N)\sum_\beta e^{i\beta\lambda n}\langle\beta_{\rm reg}|U_F|\beta_{\rm reg}\rangle$. In the effective approach, $\langle\beta_{\rm reg}|U_F|\beta_{\rm reg}\rangle$ is $\exp(-i\varepsilon_{\rm reg}^{\rm eff}(\beta)\,t/\hbar_{\rm eff})$, which does not take into account the Rabi oscillations of each regular Bloch wave $|\beta_{\rm reg}\rangle$ with the chaotic sea $|\beta_{\rm ch}\rangle$, whose amplitude is given in a two-level approximation by $W/\sqrt{W^2+\Delta^2}$ and whose period is $\pi\hbar_{\rm eff}/\sqrt{W^2+\Delta^2}$ (Δ being the energy difference with the chaotic state involved). The effective picture is thus valid since (i) the sharpness of resonances guarantees that the total part of the system that is delocalized in the chaotic sea is small at any time (the oscillation amplitude being large only close to the resonances), and (ii) the slowest Rabi oscillation is from Eq. (3) always faster than the induced tunneling process ($\hbar_{\rm eff}/|t_n^{\rm eff}| \geq \pi\hbar_{\rm eff}/W$). This is confirmed by Fig. 4(b): the projection of the system on the chaotic sea displays fast and weak oscillations around a very low value.

Experiments.—The regime of parameters we considered is experimentally relevant (lattice of depth $5E_L$ and $\nu \approx 40$ kHz as it was achieved recently [48]). Two complementary approaches could provide direct experimental signatures of long-range tunneling: the *in situ* imaging of the cloud shape dynamics and the use of Bloch oscillations generalized to amplitude modulated lattices [64,65] that provides a direct spectrometry of the band from which long-range properties could be inferred [66–68].

Conclusion.—In this Letter, we generalized the original chaos-assisted tunneling mechanism between two wells to spatially periodic lattice systems. We demonstrated that in an intermediate regime of temporal driving, the system dynamics could be mapped onto a tight-binding Hamiltonian with long-range hopping. This is a direct consequence of the existence of sharp tunneling resonances in the band structure [48]. These properties are a generic and robust feature of driven lattices whose classical dynamics is mixed. This effect could thus be observed in many different experimental situations.

Our study opens new possibilities for quantum simulation. First, the versatility of mixed systems allows one to engineer more complex Hamiltonians such as a chain of dimers with long-range hoppings (with two islands per cell, see [48]), i.e., an extended Su-Schrieffer-Heeger model that

features nontrivial topological properties [69]. Second, long-range hoppings in disordered lattices can generically induce nonergodic delocalized states with multifractal properties (like in power-law random banded matrices [12]). Hence by adding disorder in the system, this framework should provide a way to experimentally observe quantum multifractality [70], which is very challenging to achieve by other means [71–74]. Finally, a proper description of many-body effects in such systems is still missing, but we may expect that they only appear within the regular islands (where the density is high) mimicking Hubbard on-site interactions. This could allow one to access experimentally many-body localization and spin glass physics, where long-range tunnelings play an important role [10,75,76].

This work was supported through the EUR Grant NanoX No. ANR-17-EURE-0009 in the framework of the "Programme des Investissements d'Avenir," and research funding Grant No. ANR-17-CE30-0024. We thank Calcul en Midi-Pyrénées (CALMIP) for computational resources and assistance. We thank O. Gauthé and B. Peaudecerf for useful discussions.

[1] I. Bloch, J. Dalibard, and S. Nascimbène, Nat. Phys. **8**, 267 (2012).
[2] R. Blatt and C. F. Roos, Nat. Phys. **8**, 277 (2012).
[3] A. Aspuru-Guzik and P. Walther, Nat. Phys. **8**, 285 (2012).
[4] J. W. Britton, B. C. Sawyer, A. C. Keith, C.-C. J. Wang, J. K. Freericks, H. Uys, M. J. Biercuk, and J. J. Bollinger, Nature (London) **484**, 489 (2012).
[5] R. Landig, L. Hruby, N. Dogra, M. Landini, R. Mottl, T. Donner, and T. Esslinger, Nature (London) **532**, 476 (2016).
[6] C.-L. Hung, A. González-Tudela, J. I. Cirac, and H. J. Kimble, Proc. Natl. Acad. Sci. U.S.A. **113**, E4946 (2016).
[7] H. Busche, P. Huillery, S. W. Ball, T. Ilieva, M. P. A. Jones, and C. S. Adams, Nat. Phys. **13**, 655 (2017).
[8] V. M. Bastidas, T. Haug, C. Gravel, L. C. Kwek, W. J. Munro, and K. Nemoto, arXiv:2009.00823.
[9] M. M. Roses, H. Landa, and E. G. D. Torre, arXiv:2102.09590.
[10] D. Sherrington and S. Kirkpatrick, Phys. Rev. Lett. **35**, 1792 (1975).
[11] R. M. Nandkishore and S. L. Sondhi, Phys. Rev. X **7**, 041021 (2017).
[12] A. D. Mirlin, Y. V. Fyodorov, F.-M. Dittes, J. Quezada, and T. H. Seligman, Phys. Rev. E **54**, 3221 (1996).
[13] A. Eckardt, Rev. Mod. Phys. **89**, 011004 (2017).
[14] N. H. Lindner, G. Refael, and V. Galitski, Nat. Phys. **7**, 490 (2011).
[15] M. C. Rechtsman, J. M. Zeuner, Y. Plotnik, Y. Lumer, D. Podolsky, F. Dreisow, S. Nolte, M. Segev, and A. Szameit, Nature (London) **496**, 196 (2013).
[16] N. Goldman and J. Dalibard, Phys. Rev. X **4**, 031027 (2014).
[17] I.-D. Potirniche, A. C. Potter, M. Schleier-Smith, A. Vishwanath, and N. Y. Yao, Phys. Rev. Lett. **119**, 123601 (2017).
[18] N. R. Cooper, J. Dalibard, and I. B. Spielman, Rev. Mod. Phys. **91**, 015005 (2019).
[19] G. Casati, B. V. Chirikov, F. M. Izraelev, and J. Ford, in *Stochastic Behavior in Classical and Quantum Hamiltonian Systems*, Lecture Notes in Physics Vol. 93, edited by G. Casati and J. Ford (Springer-Verlag, Berlin/Heidelberg, 1979), pp. 334–352.
[20] S. Fishman, D. R. Grempel, and R. E. Prange, Phys. Rev. Lett. **49**, 509 (1982).
[21] R. Graham, M. Schlautmann, and D. L. Shepelyansky, Phys. Rev. Lett. **67**, 255 (1991).
[22] F. L. Moore, J. C. Robinson, C. F. Bharucha, B. Sundaram, and M. G. Raizen, Phys. Rev. Lett. **75**, 4598 (1995).
[23] G. Casati, I. Guarneri, and D. L. Shepelyansky, Phys. Rev. Lett. **62**, 345 (1989).
[24] J. Chabé, G. Lemarié, B. Grémaud, D. Delande, P. Szriftgiser, and J. C. Garreau, Phys. Rev. Lett. **101**, 255702 (2008).
[25] A. R. Kolovsky, S. Miyazaki, and R. Graham, Phys. Rev. E **49**, 70 (1994).
[26] S. Tomsovic and D. Ullmo, Phys. Rev. E **50**, 145 (1994).
[27] O. Bohigas, S. Tomsovic, and D. Ullmo, Phys. Rep. **223**, 43 (1993).
[28] F. Leyvraz and D. Ullmo, J. Phys. A **29**, 2529 (1996).
[29] A. Shudo, Y. Ishii, and K. S. Ikeda, Europhys. Lett. **81**, 50003 (2008).
[30] A. Bäcker, R. Ketzmerick, M. Robnik, G. Vidmar, R. Höhmann, U. Kuhl, and H.-J. Stöckmann, Phys. Rev. Lett. **100**, 174103 (2008).
[31] A. Bäcker, R. Ketzmerick, S. Löck, and L. Schilling, Phys. Rev. Lett. **100**, 104101 (2008).
[32] S. Löck, A. Bäcker, R. Ketzmerick, and P. Schlagheck, Phys. Rev. Lett. **104**, 114101 (2010).
[33] O. Brodier, P. Schlagheck, and D. Ullmo, Phys. Rev. Lett. **87**, 064101 (2001).
[34] O. Brodier, P. Schlagheck, and D. Ullmo, Ann. Phys. (Amsterdam) **300**, 88 (2002).
[35] N. Mertig, S. Löck, A. Bäcker, R. Ketzmerick, and A. Shudo, Europhys. Lett. **102**, 10005 (2013).
[36] A. Mouchet, C. Miniatura, R. Kaiser, B. Grémaud, and D. Delande, Phys. Rev. E **64**, 016221 (2001).
[37] A. Mouchet and D. Delande, Phys. Rev. E **67**, 046216 (2003).
[38] S. Keshavamurthy and P. Schlagheck, *Dynamical Tunneling—Theory and experiment* (CRC Press, Boca Raton, 2011).
[39] C. Dembowski, H.-D. Gräf, A. Heine, R. Hofferbert, H. Rehfeld, and A. Richter, Phys. Rev. Lett. **84**, 867 (2000).
[40] R. Hofferbert, H. Alt, C. Dembowski, H.-D. Gräf, H. L. Harney, A. Heine, H. Rehfeld, and A. Richter, Phys. Rev. E **71**, 046201 (2005).
[41] S. Gehler, S. Löck, S. Shinohara, A. Bäcker, R. Ketzmerick, U. Kuhl, and H.-J. Stöckmann, Phys. Rev. Lett. **115**, 104101 (2015).
[42] S. Shinohara, T. Harayama, T. Fukushima, M. Hentschel, T. Sasaki, and E. E. Narimanov, Phys. Rev. Lett. **104**, 163902 (2010).
[43] M.-W. Kim, S. Rim, C.-H. Yi, and C.-M. Kim, Opt. Express **21**, 32508 (2013).
[44] B. Dietz, T. Guhr, B. Gutkin, M. Miski-Oglu, and A. Richter, Phys. Rev. E **90**, 022903 (2014).

[45] W. K. Hensinger, H. Häffner, A. Browaeys, N. R. Heckenberg, K. Helmerson, C. McKenzie, G. J. Milburn, W. D. Phillips, S. L. Rolston, H. Rubinsztein-Dunlop, and B. Upcroft, Nature (London) **412**, 52 (2001).
[46] D. A. Steck, Science **293**, 274 (2001).
[47] D. A. Steck, W. H. Oskay, and M. G. Raizen, Phys. Rev. Lett. **88**, 120406 (2002).
[48] M. Arnal, G. Chatelain, M. Martinez, N. Dupont, O. Giraud, D. Ullmo, B. Georgeot, G. Lemarié, J. Billy, and D. Guéry-Odelin, Sci. Adv. **6**, eabc4886 (2020).
[49] K. Vant, G. Ball, H. Ammann, and N. Christensen, Phys. Rev. E **59**, 2846 (1999).
[50] J.-B. Shim, S.-B. Lee, S. W. Kim, S.-Y. Lee, J. Yang, S. Moon, J.-H. Lee, and K. An, Phys. Rev. Lett. **100**, 174102 (2008).
[51] Y.-F. Xiao, X.-F. Jiang, Q.-F. Yang, L. Wang, K. Shi, Y. Li, and Q. Gong, Laser Photonics Rev. **7**, L51 (2013).
[52] Q.-F. Yang, X.-F. Jiang, Y.-L. Cui, L. Shao, and Y.-F. Xiao, Phys. Rev. A **88**, 023810 (2013).
[53] R. Dubertrand, J. Billy, D. Guéry-Odelin, B. Georgeot, and G. Lemarié, Phys. Rev. A **94**, 043621 (2016).
[54] $p = 2\pi P/(M\omega d)$, $x = 2\pi X/d$, where P and X are the momentum and position along the optical lattice, M is the atomic mass, d is the lattice spacing, and the time t is measured in units of the modulation angular frequency ω.
[55] M. V. Berry, J. Phys. A **10**, 2083 (1977).
[56] K. Husimi, Proc. Phys.-Math. Soc. Jpn. **22**, 264 (1940).
[57] M. Terraneo, B. Georgeot, and D. L. Shepelyansky, Phys. Rev. E **71**, 066215 (2005).
[58] S.-J. Chang and K.-J. Shi, Phys. Rev. A **34**, 7 (1986).
[59] H. Feshbach, Ann. Phys. (N.Y.) **5**, 357 (1958).
[60] H. Feshbach, Ann. Phys. (N.Y.) **19**, 287 (1962).
[61] P. Löwdin, J. Math. Phys. (N.Y.) **3**, 969 (1962).
[62] See Supplemental Material, which includes Refs. [48, 57], at http://link.aps.org/supplemental/10.1103/PhysRevLett.126.174102 for computational details, an analytical derivation of the hopping law, Eq. (3), and extended data (with smaller $\hbar_{\text{eff}}$ and for different classical transports).
[63] P. Beckmann, J. Res. Natl. Bur. Stand. **66D**, 231 (1962).
[64] Z. A. Geiger, K. M. Fujiwara, K. Singh, R. Senaratne, S. V. Rajagopal, M. Lipatov, T. Shimasaki, R. Driben, V. V. Konotop, T. Meier, and D. M. Weld, Phys. Rev. Lett. **120**, 213201 (2018).
[65] C. J. Fujiwara, K. Singh, Z. A. Geiger, R. Senaratne, S. V. Rajagopal, M. Lipatov, and D. M. Weld, Phys. Rev. Lett. **122**, 010402 (2019).
[66] J. Stockhofe and P. Schmelcher, Phys. Rev. A **91**, 023606 (2015).
[67] F. Dreisow, G. Wang, M. Heinrich, R. Keil, A. Tünnermann, S. Nolte, and A. Szameit, Opt. Lett. **36**, 3963 (2011).
[68] G. Wang, J. P. Huang, and K. W. Yu, Opt. Lett. **35**, 1908 (2010).
[69] B. Pérez-González, M. Bello, Álvaro Gómez-León, and G. Platero, arXiv:1802.03973.
[70] F. Evers and A. D. Mirlin, Rev. Mod. Phys. **80**, 1355 (2008).
[71] S. Faez, A. Strybulevych, J. H. Page, A. Lagendijk, and B. A. van Tiggelen, Phys. Rev. Lett. **103**, 155703 (2009).
[72] A. Richardella, P. Roushan, S. Mack, B. Zhou, D. A. Huse, D. D. Awschalom, and A. Yazdani, Science **327**, 665 (2010).
[73] R. Dubertrand, I. García-Mata, B. Georgeot, O. Giraud, G. Lemarié, and J. Martin, Phys. Rev. Lett. **112**, 234101 (2014).
[74] R. Dubertrand, I. García-Mata, B. Georgeot, O. Giraud, G. Lemarié, and J. Martin, Phys. Rev. E **92**, 032914 (2015).
[75] S. Nag and A. Garg, Phys. Rev. B **99**, 224203 (2019).
[76] S. J. Thomson and M. Schiró, Phys. Rev. Research **2**, 043368 (2020).